Lawrence Berkeley National Laboratory
Recent Work

Title
Seamless joining of silicon nitride ceramics

Permalink

Journal
Journal of the American Ceramic Society, 84(4)

Author
Gopal, Mani

Publication Date
2000-04-10

ERNEST ORLANDO LAWRENCE BERKELEY NATIONAL LABORATORY

Seamless Joining of Silicon Nitride Ceramics

Mani Gopal, Mark Sixta, Lutgard De Jonghe, and Gareth Thomas

Materials Sciences Division
Center for Advanced Materials

April 2000

DISCLAIMER

Seamless Joining of Silicon Nitride Ceramics

Mani Gopal, Mark Sixta, Lutgard De Jonghe,
and Gareth Thomas

Department of Materials Science and Mineral Engineering
University of California, Berkeley

and

Center for Advanced Materials
Materials Sciences Division
Ernest Orlando Lawrence Berkeley National Laboratory
University of California
Berkeley, California 94720

April 2000

Seamless Joining of

Silicon Nitride Ceramics

Mani Gopal[#,*], Mark Sixta[*], Lutgard De Jonghe[*] and Gareth Thomas

Department of Materials Science and Mineral Engineering
University of California, Berkeley CA 94720
and
Center for Advanced Materials
Lawrence Berkeley National Laboratory, Berkeley, CA 94720

Abstract

High-strength joining of Si_3N_4 ceramics has been achieved using an interlayer of a rare-earth silicate sintering aid. The process effectively eliminates the seam, and may allow for fabrication of large or complex silicon nitride bodies. This approach to joining is based on the concept that when sintering aids are effective in bonding individual grains, they could be equally effective in joining bulk pieces of Si_3N_4. Optimization of the process led to Si_3N_4/Si_3N_4 joints with room temperature bend strengths as high as 950 MPa, corresponding to more than 90% the bulk strength of the Si_3N_4. At elevated temperatures of 1000°C and 1200°C joint strengths of 666 and 330 MPa, respectively, were obtained, which are the highest values reported to date for these temperatures.

[#] Presently at the Department of Materials Science and Engineering, Massachusetts Institute of Technology, Cambridge, MA 02139
[*] Member, American Ceramic Society

These bend strengths are also more that 90% of the strength of bulk Si_3N_4 measured at these temperatures.

I. Introduction

Joining of and ceramics, including silicon nitride, has been the subject of numerous investigations [1-6]. Most of the approaches to joining involve the use of an interlayer, which can be a ceramic, a polymeric precursor, a metallic alloy, or some combination of these [7-10].

Joining Si_3N_4 ceramics using sintering aids as the interlayer was first developed by Loehman *et al.* [11-12]. The rationale behind this approach is that if these sintering aids produce good bonding between individual grains, they should also be suitable for bonding bulk material. The excellent physical and chemical compatibility achieved in the bulk between the grain and the grain boundary phase should extend to similar bulk-joint interfaces. The joints thus produced have good room temperature [13] and high temperature properties [14]. After the initial development work, a number of workers persued the idea and varied the sintering aid composition to effect joining [15-20]. However, there has not yet been a systematic study of the microstructural evolution of the joint. The purpose of this paper is to provide guidelines to optimize such joining, and in the process, to unify the work of the other groups.

Our approach to joining is to use sintering aids that will impart the best high temperature properties to bulk Si_3N_4 and consequently to the joint. The common feature of the above mentioned approaches is the use of Al_2O_3 as a component of the interlayer. While the use of Al_2O_3 permits sintering at lower temperatures, it also promotes the retention of glassy phases between the Si_3N_4 grains [21]. The choice of sintering aid utilized in this work is based on the earlier work of Cinibulk *et al.* [22], who sintered Si_3N_4 powders with a mixture of rare-earth oxide (RE_2O_3) and silica (SiO_2). When the chemistry and sintering schedule is carefully controlled, the intergranular phase is the crystalline $RE_2Si_2O_7$ phase, which imparts improved mechanical and oxidation properties to the Si_3N_4. By analogy with the results for sintered compacts, it is proposed that bulk Si_3N_4 joined with the same rare-earth silicate glass should also have similar better properties.

II. Background

(1) Silicon nitride sintering

As will be discussed later, the mechanism by which ceramic joining is achieved is similar to that by which silicon nitride sinters. An understanding of the microstructural evolution follows from a consideration of the sintering mechanisms in silicon nitride. A brief review of these mechanisms is presented here, and further details can be found elsewhere [23-24]. To densify Si_3N_4, it is necessary to form a liquid phase at high temperatures which requires the use of sintering aids that are typically a mixture of various oxides including

silica. At high temperatures, the oxides mix and form a silicate flux, which assists in the densification process [25]. The densification process, which occurs above 1900°C, also induces a phase change causing the material to transform from the low-temperature α-Si_3N_4 to the high-temperature β-Si_3N_4. This densification and transformation occurs by the dissolution of α-Si_3N_4 grains into the silicate flux followed by re-precipitation as β-Si_3N_4 on other pre-existing grains [26]. The growing Si_3N_4 grains reject the silicate flux that forms the intergranular phase. The final microstructure therefore consists of needle-like grains of β-Si_3N_4, equiaxed α-Si_3N_4 plus the intergranular phase.

The increase in toughness of Si_3N_4 is due to the formation of these elongated β-Si_3N_4 grains [27]. During fracture, the elongated grains pull out and bridge the crack, thereby shielding the crack tip from the applied load. While the grains control the toughness, the high temperature strength is limited by the decreased viscosity of the intergranular phase. Detailed analysis by Cinibulk *et al.* has shows that the desired grain boundary phase is a rare-earth disilicate ($RE_2Si_2O_7$). Si_3N_4 sintered to obtain this phase has the best creep, oxidation and high-temperature strength [28-29]. Consequently, this material has been chosen as the interlayer for joining Si_3N_4.

(2) Silicon nitride joining

The starting composition of the interlayer glass is 2 parts RE_2O_3 and 1 part SiO_2, which react to form the desired $RE_2Si_2O_7$ composition. During heating, the compounds react to

form transient intermediate phases prior to the formation of the final phase. The formation of these transient phases permits the processing at relatively low temperatures using the phenomenon of sub-eutectic densification [30]. In the Yb_2O_3-SiO_2 system, the melting point of $Yb_2Si_2O_7$ is 1850°C [31], which is the temperature above which Si_3N_4 powders are typically sintered. For joining, utilizing the deep eutectic present near the disilicate phase (at 1650°C for $Yb_2Si_2O_7$ [31]) lowers the processing temperature. Above this eutectic temperature, a sufficient amount of transient liquid is formed to cause wetting. Subsequent inter-diffusion causes the formation of the phase determined by the initial stoichiometry, viz. $RE_2Si_2O_7$. A mixture of two rare-earth disilicates, which form a eutectic, further lowers the joining temperature [32]. The eutectic reaction takes place at a temperature that is about 150°C to 200°C lower than that of the pure disilicate phase. The onset of liquid formation could occur as low as 1450-1550°C depending on the rare-earth oxide used.

III. Experimental Approach

(1) Joining methods

For the joining experiments, bulk Si_3N_4 specimens (Toshiba Corporation) were ground to a surface finish of ~40 μm. The interlayer was prepared by mixing commercial Y_2O_3, Yb_2O_3 and SiO_2 powders. Since the powders are hygroscopic, they were heated to 500°C to remove adsorbed moisture. Subsequently, Y_2O_3, Yb_2O_3 and SiO_2 powders were weighed such that the overall composition was $(Y_2O_3 + Yb_2O_3).2SiO_2$. The powders were

then milled in an attritor mill in 2-propanol, with YSZ balls as the grinding medium. The slurry was dried, and the powders ground to pass through 325 mesh sieve ($\sim 40 \mu m$).

The dried powders were cold pressed to form pellets, and were inserted between the two pieces of Si_3N_4. Depending on the amount of powder used, the pellets should densify to form 15 to 150 μm thick layers (if no reaction were to occur). However, as will be discussed later, the thickness of the starting interlayer does not affect the final microstructure. The specimen was placed inside a boron nitride crucible and Si_3N_4 powder added around the specimens to form a bed. In addition, N_2 atmosphere was used to minimize decomposition reactions.

A very important consideration in the experimental setup is the absence of constraint on the sides of the specimens (Figure 1). This permits any excess interlayer material to flow out upon liquefaction. Joining was effected by heating the specimens at 5°C per minute to a temperature between 1400 to 1900°C, holding for 0 to 4 hours, followed by cooling at 2°C per minute. During the joining process, a small pressure ($\sim$0.01 to 0.1 MPa) was applied to maintain interfacial contact.

(2) Microstructure analysis

As will be shown later, the joint region could not be distinguished from the bulk in the optimized microstructure. The location of the joint could be determined from the offsets at the ends of the specimens, or from small regions of porosity in the joint. Low magnification optical and TEM images were taken, and used as maps to ensure that the

observations were being made on the joint region. In a few specimens, there was a difference in the polishing rates of the joint and the bulk due to differences in the grain size, residual porosity or residual glass in the joint. This caused the formation of a small groove on the polished surface, which can be seen under grazing incident light, and in some SEM images.

Transmission electron microscopy (TEM) was used to characterize the microstructure of the joint and bulk regions. The specimens were prepared using conventional dimpling and ion milling methods. The ion-milling process was kept to a minimum, to minimize preferential etching of the joint region. Upon ion milling, the specimens were coated with a thin layer of carbon and analyzed in the TEM (Philips 400 EM and JEOL 200CX).

Scanning electron microscopy (ISI - D130C) was used to character the structure and chemistry of the joint region. The microstructure was studied by etching the specimens in molten KOH for 1-2 minutes. This etching process removed the grain boundary phases, revealing the distribution of grains in the joint and bulk regions. The microstructure was studied using secondary and back-scattered electrons. In addition, spectroscopic analysis was performed on specimens that were polished to a surface finish of 1 μm. The techniques used included both energy dispersive (EDS) and wavelength dispersive spectroscopy (WDS).

(3) Mechanical properties

The joining process was optimized for best mechanical properties using indentation techniques. The specimens were cut perpendicular to the joint, and polished to a surface finish 3 μm. A Vickers indenter was used to initiate cracks both in the bulk region and near the joint. The distance of the indent from the interface and the angle between the crack and interface were carefully controlled to permit accurate analysis. Upon optimization using this approach, larger pieces of bulk Si_3N_4 were joined to determine the bend strengths. Beams of approximately 3 x 3 x 28 mm were sectioned from the Si_3N_4 pieces joined at various conditions. The tensile surfaces of the bend bars were polished to a 1 μm surface finish, and the edges were beveled on a 6 μm diamond wheel to reduce edge flaws. The specimens were broken on a four-point bending jig to determine the flexural strength.

IV. Results and Discussion

(1) Microstructure Evolution

(1) Observed microstructures

The observed microstructure of the joints can be classified into three broad categories - (a) joints with residual glass, (b) joints with residual porosity and (c) seamless joints. Figure 2 (a) is a bright field TEM image of the specimen with glass in the joint. The dark band corresponds to the regions where there is residual glass, which because of its higher atomic mass, is a stronger electron absorber as compared to the bulk Si_3N_4 and so has

dark contrast. Figure 2 (b) is a optical image of the same specimen, with the glassy joint in bright contrast. The second category of specimens are those in which there is residual porosity, and can be seen in the optical micrograph in Figure 3. The third category are those in which the joint region cannot be distinguished from the bulk. Figures 4 (a) and (b) are SEM images of specimen that have been polished and etched in molten KOH (at about 360°C) for 1 minute. The images have been taken near regions of porosity, to prove that these are images from the joint regions. As can be seen from the images, the microstructure of the joint region is remarkably similar to that of the joint region. Figure 5 is a dark-field TEM image taken from the joint region, with the direction of the joint shown by the arrows in the corners. This microstructure is very similar to that found in bulk Si_3N_4, with elongated β-Si_3N_4 grains providing the toughening.

The distribution of cations in the bulk and joint region was analyzed by both wavelength dispersive (WDS) and energy dispersive spectroscopy (EDS) in the SEM, and EDS in the TEM. The WDS line scans done on the polished specimen shows that the concentration of cations in the joint is similar to that of the bulk, and that any chemical gradients could not be resolved [33]. This is expected because quantitative analytical measurements by other groups have shown that the cations present in the interlayer diffuse by as much as 90 μm into the bulk via the intergranular phase [14].

(2) Analysis of microstructure evolution

When the specimens processed under various conditions are plotted in a temperature-time map, the three observed microstructures fall into the regions shown schematically in Figure 6. The low temperature and short time regime corresponds to regions of remnant glass. The high temperature and long time regime corresponds to regions of residual porosity. In the middle, is the region where the microstructure is optimized, and seamless joints of silicon nitride can be produced.

The factors controlling the observed microstructure evolution are (a) squeezing out of the excess glass by the applied load, (b) dissolution and re-precipitation of Si_3N_4, (c) diffusion of glass into the bulk and (d) rearrangement of the microstructure. Of these mechanisms, the squeezing out of the glass and the diffusion of the glass into the bulk control the glass content of the joint. The other two mechanisms, dissolution/re-precipitation and rearrangement of the grains control the grain size and its distribution in the joint.

During the joining process, the rare-earth oxide reacts with silica to form a liquid silicate flux. This liquid silicate is squeezed out from the joint by the applied load. The amount of liquid squeezed out is dependent on the capillary forces and the viscosity of the glass, which in turn are dependent on its chemistry and the processing temperature. Simultaneously, the Si_3N_4 grains present on the surface dissolve into this silicate flux. The β-Si_3N_4 grains, which precipitate from the silicate flux, nucleates on existing Si_3N_4

grains present on the surface of the bulk, and grow out into the glass as no microstructural constraints exist in that direction. These needle-like β-Si_3N_4 grains that have grown into the interlayer also mechanically trap some of the glass. It is in these trapped pockets of glass that additional precipitation of β-Si_3N_4 occurs.

The two other processes mentioned earlier are also involved in the microstructural evolution. One of these is microstructural re-arrangement, which occurs because all the grains are not attached to the bulk Si_3N_4[18]. The other process is the diffusion of glass into the bulk Si_3N_4. This occurs via grain boundary diffusion, with the cations diffusing as much as 90 μm into the bulk[14].

When the processing temperature is low and / or the time is short (such as at 1600°C for 30 minutes), the glass that is present initially is not fully removed either by squeezing out or by diffusion into the bulk. Consequently, the joint region has residual glass in it. When the processing temperature is high and/or the time is long (such as at 1700°C for 120 minutes), the viscosity of the glass is low and the diffusion coefficients are high. Hence, too much of the glass is removed from the joint region resulting in porosity. When the processing time and temperature are optimized (at 1650°C for 60 minutes), an optimal amount of glass is removed resulting in the "elimination" of the joints.

It should be noted that there are other conditions, indicated by the band in figure 6, where there is no residual glass. However, under these conditions, the grain size distribution in

the joint region is different from that in the bulk. This results in a difference in mechanical properties, such as variation in wear resistance as evidenced during polishing.

(3) Comparison with work by other groups

In the early work, when a MgO-Al$_2$O$_3$-SiO$_2$ glass was used to join at temperatures between 1550°C and 1650°C, a distinct glassy interlayer was found [11-12, 14]. The thickness of the joint ranged from ~10 µm to ~120 µm. Although most of the interlayer was glassy, needle-like grains of Si$_2$N$_2$O and β-Si$_3$N$_4$ were observed at the interface between the bulk Si$_3$N$_4$ and the interlayer. In a different study, a mixture of Si$_3$N$_4$, Y$_2$O$_3$, Al$_2$O$_3$ and SiO$_2$ was used to join Si$_3$N$_4$ at 1600°C [18-19]. Upon joining, the interlayer was found to consist of β-SiAlON grains in a glassy matrix. The thickness of the joint was estimated to be between 1 µm and 2 µm. The above mentioned studies show that as the thickness of the interlayer decreases, the fraction of crystalline grains present increases. This is consistent with our observation - as the thickness becomes "zero", the crystallinity of the interlayer becomes similar to that in bulk Si$_3$N$_4$. In other words, the original interface is consumed by the reaction.

The second observation seen by other groups is the formation of Si$_2$N$_2$O. These acicular grains grow out from the surface of the bulk into the glass and span the joint [11, 14]. Detailed analysis of the chemical reactions at these high temperatures [13] shows that Si$_2$N$_2$O is not the thermodynamically favored phase. Instead, they are formed due to local chemical gradients induced by the dissolution of the Si$_3$N$_4$ grains from the surface of the

bulk. Upon processing for longer times, the Si_2N_2O dissolves back into the glass. In the experiments performed, the joining time was 60 minutes, which is sufficiently long to obtain equilibrium. The Si_2N_2O grains are therefore not observed in these experiments.

(2) Properties of the joint

(1) Oxidation

The oxidized specimens were analyzed using the SEM. As discussed in an earlier paper [34], the oxide scale about the joint regions was much smaller than that above the bulk Si_3N_4. This shows that the oxidation resistance of the joint is superior to that of the bulk Si_3N_4 (which was sintered using conventional sintering aids).

(2) Toughness

Indentation was used to characterize qualitatively the toughness of the joint [35]. As discussed in an earlier paper [33], these results could be used as a guide for optimizing the processing condition. The approach is based on a fracture mechanics analysis of crack deflection at interfaces [36-37]. These analyses consider the energies for deflection and penetration through the interface. When a crack impinges on the interface at a high angle, interface penetration is energetically favored. When the angle of incidence is shallow, crack deflection is favored. The angle at which the transition occurs from penetration to deflection, is a measure of the toughness of the interface [38]. The specimens with the highest toughness were then tested for room-temperature and high-temperature strength.

(3) Strength

The strengths of the joints have been measured using 4-point bending methods. The as-received bulk Si_3N_4 has an average strength of 1013 MPa as indicated in Table 1.

Table 1
Room temperature strength of bulk Si_3N_4.

Testing temperature (°C)	Number of beams tested	Average strength (MPa)	Standard deviation (MPa)	Maximum strength (MPa)
25	4	1013	25	1031

Table 2
Room temperature strength as a function of the joining temperature.
The holding time was 1 hour.

Joining temperature (°C)	Number of beams tested	Average strength (MPa)	Standard deviation (MPa)	Maximum strength (MPa)
1600	9	740	117	918
1650	9	937	105	1040
1700	9	816	138	994

Table 2 and Figure 7 shows room temperature bend strengths of the joined specimens plotted as a function of the joining temperature. As can be seen, the peak strength is obtained when the joining temperature is 1650°C.

Table 3
Room temperature strength as a function of joining time.
The holding temperature was 1650°C.

Joining time (hours)	Number of beams tested	Average strength (MPa)	Standard deviation (MPa)	Maximum strength (MPa)
0	9	791	109	897
1	9	937	105	1040
2	7	551	169	790

Table 3 and Figure 8 shows the bend strength as a function of the joining time. The best strength is when the holding time is 60 minutes. Longer and shorter holding times cause a decrease in strength, as discussed earlier.

Table 4
Bend strength of the joint at different testing temperature.
The specimens were joined at 1650°C for 1 hour.

Testing temperature (°C)	Number of beams tested	Average strength (MPa)	Standard deviation (MPa)	Maximum strength (MPa)
25	9	937	105	1040
1000	5	666	76	768
1200	4	340	37	389

Table 5
Bend strength of bulk Si_3N_4 at different testing temperature.

Testing temperature (°C)	Number of beams tested	Average strength (MPa)	Standard deviation (MPa)	Maximum strength (MPa)
25	4	1013	25	1031

| 1000 | 5 | 671 | 110 | 763 |
| 1200 | 5 | 360 | 29 | 400 |

Tables 4 and 5, and Figure 9 show the high-temperature strengths of joined and bulk specimens. The specimens were joined at 1650°C for 1 hour, which gave us the maximum room temperature strength. As indicated above, the decrease in strength at high temperatures is due to the presence of aluminum oxide, which is used as a sintering aid in the bulk Si_3N_4 but is a glass stabilizer. Thus, if the bulk Si_3N_4 were to be sintered using rare-earth disilicates, it is expected that the high temperature strengths will be even higher. It is important to note that the bulk specimens were tested at these temperatures as received. They were not held at 1650°C for 1 hour, which was the condition at which the specimens were joined.

Table 6
Ratios of bend strength of the joint and bulk Si_3N_4
as a function of testing temperature.
The specimens were joined at 1650°C for 1 hour.

Testing temperature (°C)	Average **joint** strength (MPa)	Average **bulk** strength (MPa)	Ratio of joint to bulk strength
25	937	1013	0.92
1000	666	670	0.99
1200	340	360	0.94

Table 6 and Figure 10 show the ratio of the average joint strength to the average bulk strength as a function of the testing temperature. In all cases, the strength of the joints is greater than 90% the strength of the bulk specimens.

V. Summary of the joining of Si_3N_4 to Si_3N_4

The method of sintering of silicon nitride powders with rare earth disilicates has been extended to the joining of silicon nitride ceramics. The joining process can be optimized such that the structure and chemistry of the joint and the bulk are remarkably similar. This similarity, which essentially eliminates the joint is caused by (a) dissolution and re-precipitation of Si_3N_4, (b) microstructural re-arrangement caused the applied load and (c) removal of the excess glass by squeezing and by diffusion into the bulk. An optimal combination of time and temperature is needed to obtain the highest performance microstructure. Lower temperatures and shorter times cause residual glass to be present in the joint. Higher temperatures and longer times cause porosity due to the excessive diffusion of the glass into the bulk.

As a consequence of the optimization process, the 4-point bend strengths of the joints obtained from this process are comparable to that of the bulk. The average room temperature strength of the joint (937 MPa) is 92% the average strength of bulk Si_3N_4 (1041 MPa). At 1000°C, the average strength of the joint (666 MPa) is 99% that of bulk

Si$_3$N$_4$ (670 MPa). And at 1200°C, the average strength of the joint (340 MPa) is 98% that

of bulk Si$_3$N$_4$ (360 MPa). These are the highest strengths yet reported for joined Si$_3$N$_4$.

VI. Acknowledgements

VII. References

[1] Proceedings of the International Forum on Structural Ceramics Joining, *Ceram. Eng. Sci. Proc.*, **10** [11-12] (1989)

[2] Structural Ceramic Joining II, Eds. A. J. Moorhead, R. E. Loehman and S. M. Johnson, *Ceram. Trans.*, **35** (1993)

[3] M. M. Schwartz, Ceramic Joining, ASM International (1990)

[4] K. Suganuma, Y. Miyamoto and M. Koizumi, "Joining of ceramics and metals", *Ann. Rev. Mater. Sci.*, **18**, 47-73 (1988)

[5] M. L. Santella, "A review of techniques for joining advanced ceramics", *Am. Ceram. Soc. Bull.*, **71** [6], 947-954 (1992)

[6] M. G. Nicholas and D. A. Mortimer, "Ceramic/metal joining for structural applications", *Mater. Sci. Tech.*, **1**, 657-665 (1985)

[7] P. F. Becher and S. A. Halen, "Solid state bonding of Si$_3$N$_4$", *Am. Ceram. Soc. Bull.*, **58**, 582-583 (1979)

[8]   G. J. Sundberg and M. K. Ferber, "Joining of silicon nitride for heat engine applications", *Ceram. Eng. Sci. Proc.*, **10** [7-8], 823-831 (1989)

[9]   N. Iwamoto, N. Umesaki and Y. Haibara, "Silicon nitride joining with glass solder in the system $CaO-SiO_2-TiO_2$", *Yogyo Kyokaishi*, **94** [8], 1880 (1986)

[10] P. F. Becher and S. A. Halen, "Solid state bonding of Si_3N_4", *Am. Ceram. Soc. Bull.*, **58**, 582-583 (1979)

[11] R. E. Loehman, "Transient liquid phase bonding of silicon nitride ceramics", In Surfaces and Interfaces in Ceramic and Ceramic-Metal Systems, Eds. J. Pask and A. G. Evans, 701-711, Plenum Press (1981)

[12] M. L. Mecartney, R. Sinclair and R. E. Loehman, "Silicon nitride joining", *J. Am. Ceram. Soc.*, **68** [9], 472-478 (1985)

[13] S. M. Johnson and D. J. Rowcliffe, "Mechanical properties of joined silicon nitride", *J. Am. Ceram. Soc.*, **68** [9], 468-472 (1985)

[14] S. J. Glass, F. M. Mahoney, B. Quillan, J. P. Pollinger and R. E. Loehman, "Refractory oxynitride joints in silicon nitride", *Acta Mater.*, **46** [7], 2393-9 (1998)

[15] H. Tabata, S. Kanzaki and M. Nakamura, "Solid state joining of silicon nitride ceramics", In Ceramic Components for Engines, Eds. S. Somiya, E. Kanai and K. Ando, 387-393, Elsevier Applied Science (1983)

[16] M. E. Milberg, H. D. Blair, W. T. Donlon and S. S. Shinozaki, "The nature of SiAlON joints between silicon nitride bodies", *J. Mater. Sci.*, **22**, 2560-2568 (1987)

[17] R. M. Neilson and D. N. Coon, "Strength of silicon nitride - silicon nitride joints bonded with oxynitride glass", *Ceram. Eng. Sci. Proc.*, **10** [11-12], 1893-1907 (1989)

[18] P. A. Walls and M. Ueki, "Joining SiAlON ceramics using composite β-SiAlON glass adhesives", *J. Am. Ceram. Soc.*, **75** [9], 2491-2497 (1992)

[19] P. A. Walls and M. Ueki, "Mechanical properties of β-SiAlON ceramics joined using composite β-SiAlON glass adhesives", *J. Am. Ceram. Soc.*, **78** [4], 999-1005 (1995)

[20] R. D. Brittain, S. M. Johnson, R. H. Lamoreaux and D. J. Rowcliffe, "High temperature chemical phenomena affecting silicon nitride joints" *J. Am. Ceram. Soc.*, **67** [8], 522-526 (1984)

[21] G. Thomas, "Design for improved high temperature strength, creep, oxidation and fatigue resistance in Si_3N_4", In Critical Issues in the Development of High Temperature Structural Materials, Eds. N. S. Stoloff, D. J. Duquette and A. F. Gamei, 349-364, TMS Society (1993)

[22] M. K. Cinibulk, G. Thomas and S. M. Johnson, "Fabrication and secondary-phase crystallization of rare-earth disilicate silicon nitride ceramics", *J. Am. Ceram. Soc.*, **75** [8], 2037-2043 (1992)

[23] D. R. Messier and W. J. Croft, "Silicon Nitride", In <u>Preparation and Properties of Solid State Materials</u>, Vol. 7, Ed. W. R. Wilcox, 131-212, Marcel Dekker (1982)

[24] G. Ziegler, J. Heinrich and G. Wotting, "Review of relationships between processing, microstructure and properties of dense and reaction-bonded silicon nitride", *J. Mater. Sci.*, **22**, 3041-3086 (1987)

[25] R. M. German, <u>Liquid phase sintering</u>, Plenum Press (1985)

[26] P. Drew and M. H. Lewis, "The microstructures of silicon nitride ceramics during hot-pressing transformations", *J. Mater. Sci.*, **9** [2], 261-269 (1974)

[27] F. F. Lange, "Fracture toughness of Si_3N_4 as a function of the initial alpha-phase content", *J. Am. Ceram. Soc.*, **62** [7-8], 428-430 (1979)

[28] M. K. Cinibulk, G. Thomas and S. M. Johnson, "Strength and creep behavior of rare-earth disilicate-silicon nitride ceramics", *J. Am. Ceram. Soc.*, **75** [8], 2050-2055 (1992)

[29] M. K. Cinibulk, G. Thomas and S. M. Johnson, "Oxidation behavior of rare-earth disilicate-silicon nitride ceramics", *J. Am. Ceram. Soc.*, **75** [8], 2044-2049 (1992)

[30] M. N. Rahaman and L. C. De Jonghe, "Reaction sintering of zinc ferrite during constant rates of heating", *J. Am. Ceram. Soc.*, **76** [7], 1739-1744 (1993)

[31] <u>Phase diagram for Ceramists</u>, Eds. E. M. Levin, C. R. Robbins and H. F. McMurdie, Figure 2391, American Ceramic Society (1969)

[32] <u>Phase diagram for Ceramists</u>, Eds. E. M. Levin, C. R. Robbins and H. F. McMurdie, Figure 2590, 2594 and 2596, American Ceramic Society (1969)

[33] M. Gopal, L. C. De Jonghe and G. Thomas, "Silicon nitride joining using rare-earth reaction sintering", *Scripta Mater.*, **36** [4], 455-460 (1997)

[34] M. Gopal, L. C. De Jonghe and G. Thomas, "Indentation and oxidation studies on silicon nitride joints", In <u>Ceramic Joining</u>, Eds. I. E. Reimanis, C. H. Henager and A. P. Tomsia, *Ceram. Trans.*, **77**, 83-90 (1997)

[35] A. K. Bhattacharya, J. J. Petrovic and S. C. Danforth, "Indentation method for determining macroscopic fracture energy of brittle bimaterial interfaces", *J. Am. Ceram. Soc.*, **75** [2], 413-417 (1992)

[36] M. Y. He and J. W. Hutchinson, "Crack deflection at an interface between dissimilar elastic materials", *Int. J. Solids Struct.*, **25** [9], 1053-1067 (1989)

[37] A. G. Evans, B. J. Dalgleish, M. Y. He and J. W. Hutchinson, "On crack path selection and the interface fracture energy in bimaterial systems", *Acta Metal.*, **37** [12], 3249-3254 (1989)

[38] P. F. Becher, S. L. Hwang and C. H. Hsueh, "Using microstructure to attack the brittle nature of silicon nitride ceramics", *MRS Bulletin*, **20** [2], 23-27 (1995)

LIST OF FIGURES

Figure 1: Schematic sketch of the experimental set-up. Note that the interlayer is not constrained, permitting it to flow out when it liquefies.

Figure 2: (a) Bright-field TEM and (b) SEM image of a joint that has residual glass. The joint appears in dark-contrast in the TEM image as it has heavy elements such as ytterbium.

Figure 3: Optical micrograph of a specimen that shows a lot of residual porosity in the joint.

Figure 4: (a) Low-magnification and (b) high-magnification SEM images of the joint region after it has been etched in molten KOH. The images have been taken near regions of residual porosity to prove that they are images of the joint region. As can be seen, the microstructure of the joint region is remarkably similar to that of the bulk region.

Figure 5: Dark-field TEM image of an optimized joint. The direction of the joint is from the top-left to the bottom right, as indicated by the arrows.

Figure 6: Time-temperature diagram summarizing the regions from which the various micrographs were taken.

Figure 7: Four-point bend strength measured at room temperature. The specimens have been joined at 1650°C for 0, 1 and 2 hours.

Figure 8: Four-point bend strength measured at room temperature. The specimens have been joined for 1 hour at 1600, 1650 and 1700°C.

Figure 9: Four-point bend strength measured at various temperatures. The specimens have been joined at 1650°C for 1 hour. The bulk samples were tested as received, without any high-temperature heat treatment.

Figure 10: Ratio of the bend strengths of the joint specimens to the bulk specimen, as a function of testing temperature. Note that the joint specimens have strength greater than 90% the strength of the bulk specimen at all temperatures.
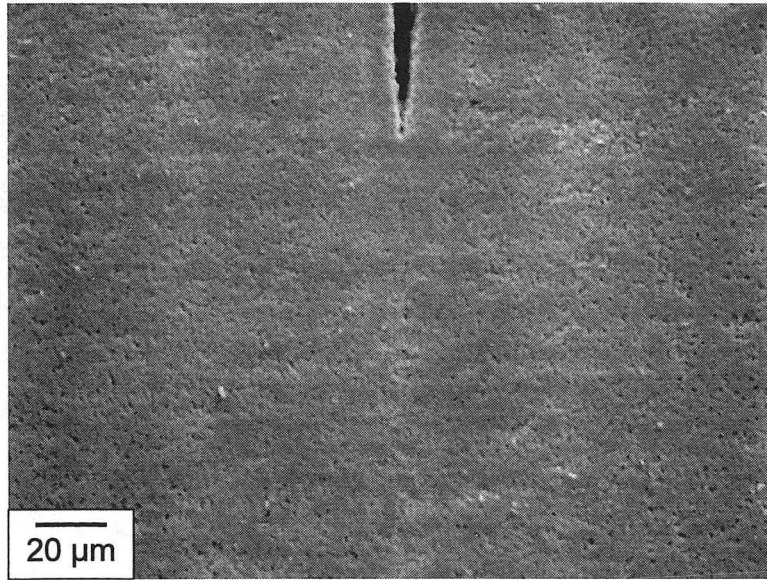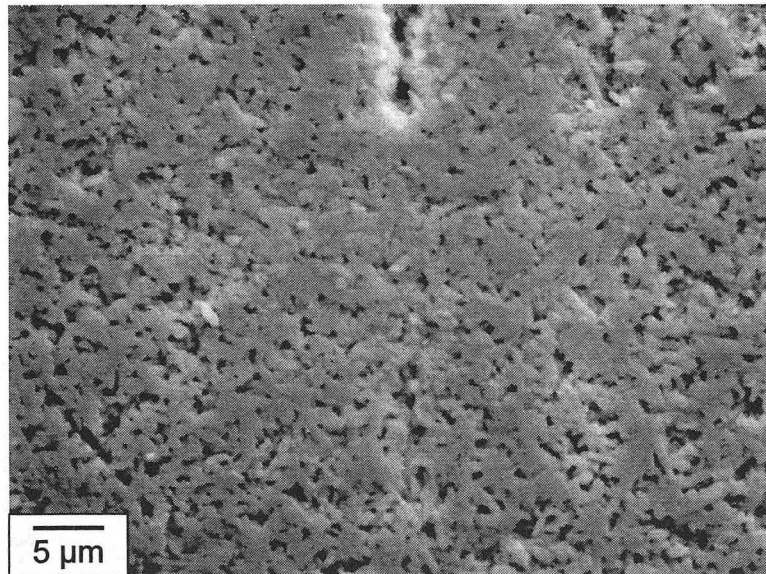
Figure 1

1 μm
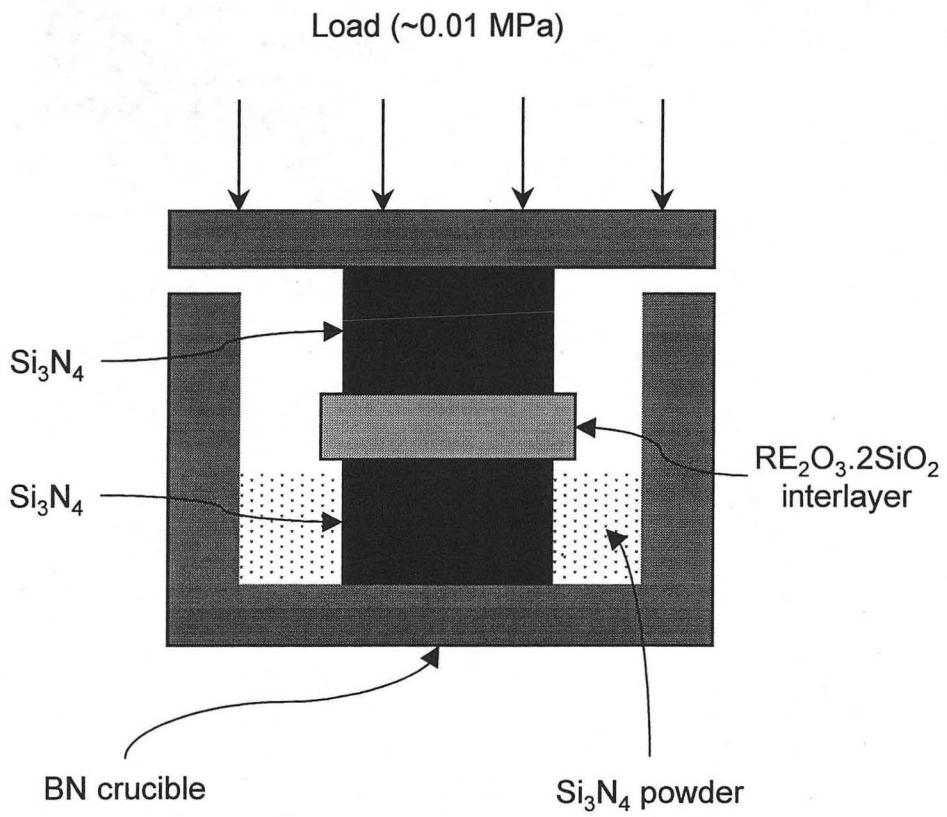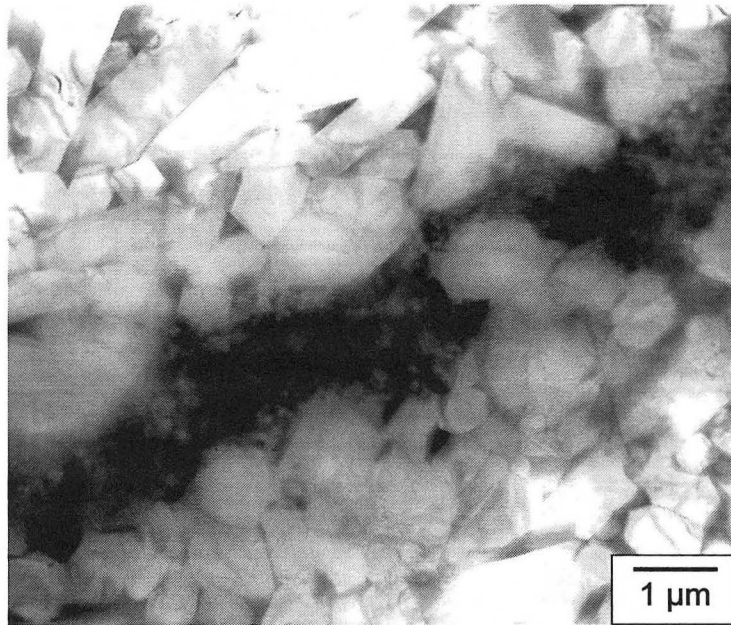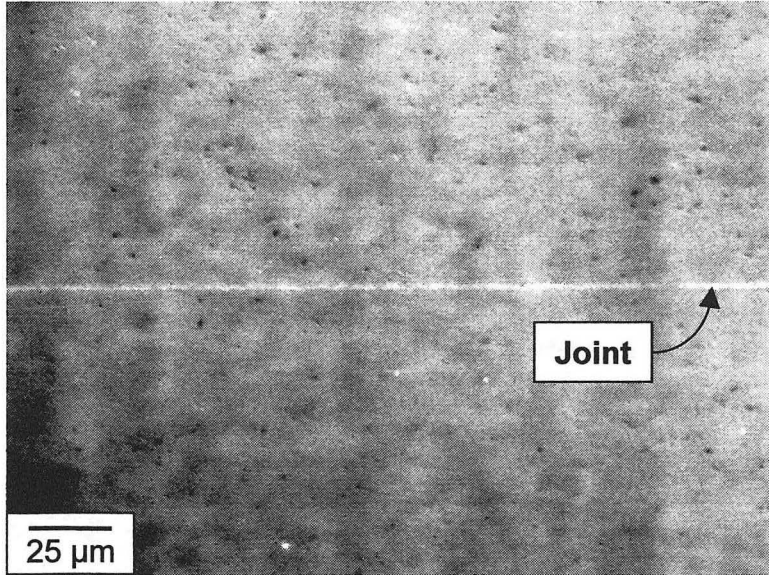
Figure 2 (a)

Figure 2(b)
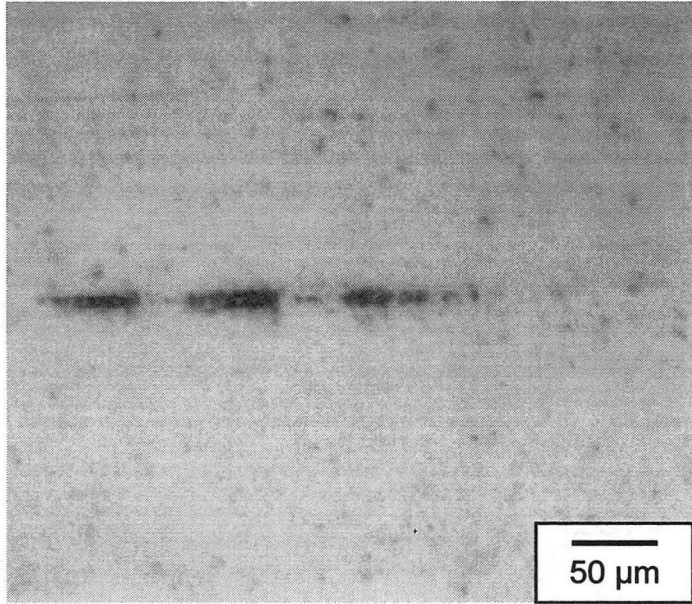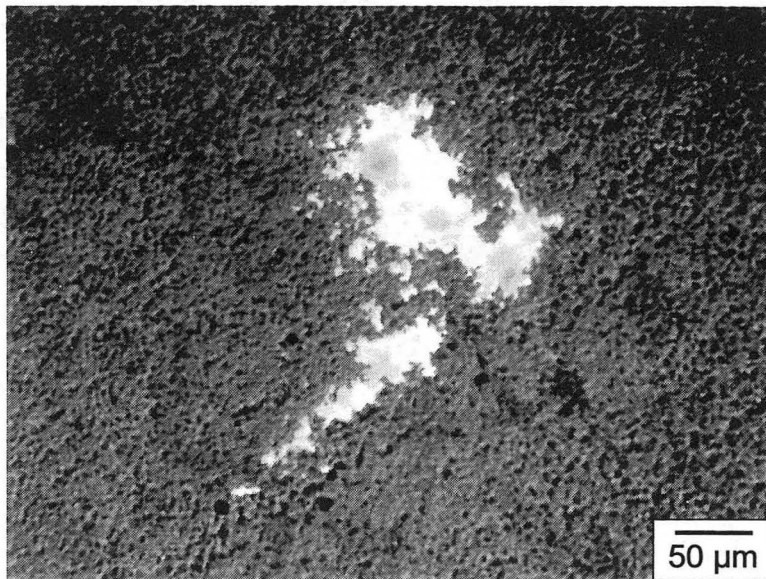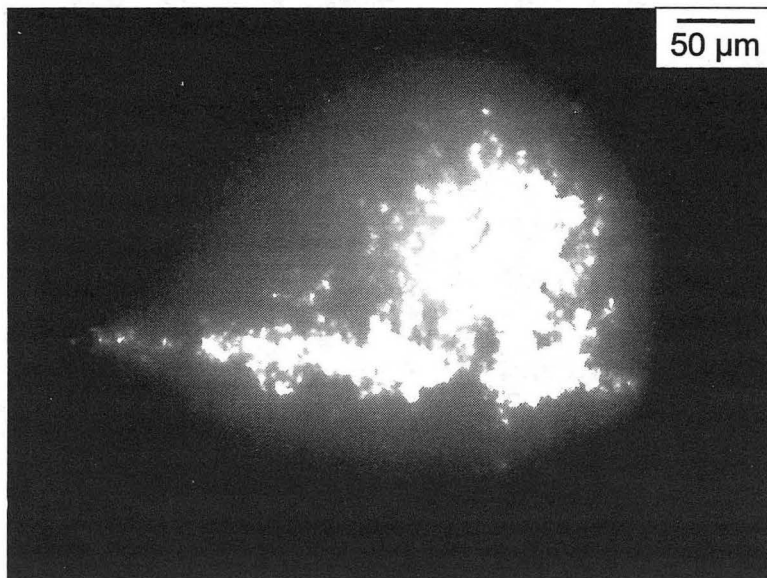
Figure 3

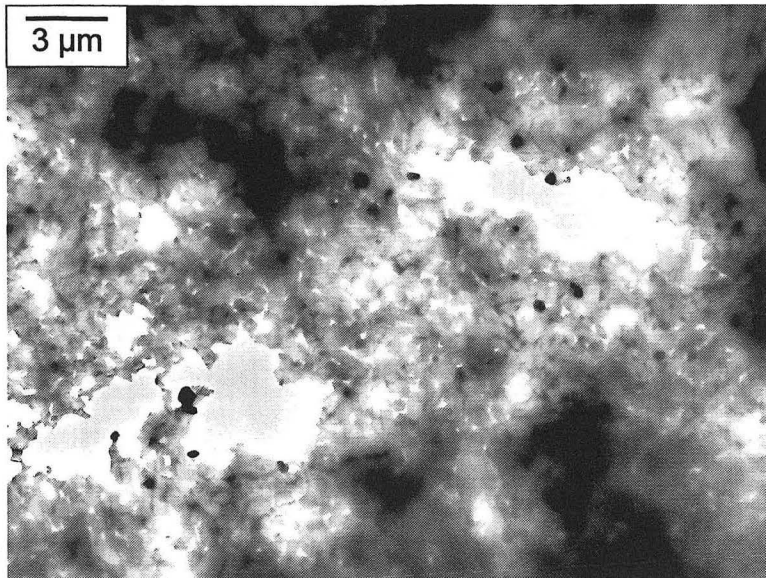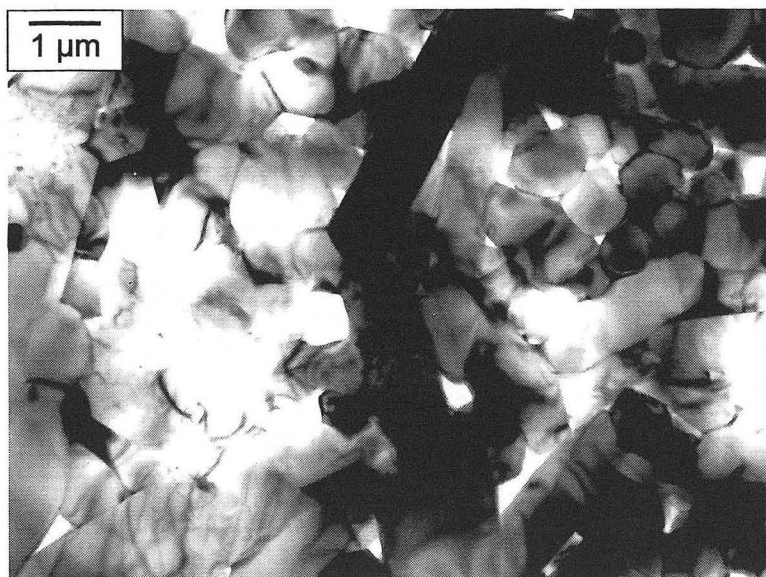**Figure 4 (a)**

Figure 4 (b)

Figure 5 (a)

Figure 5 (b)
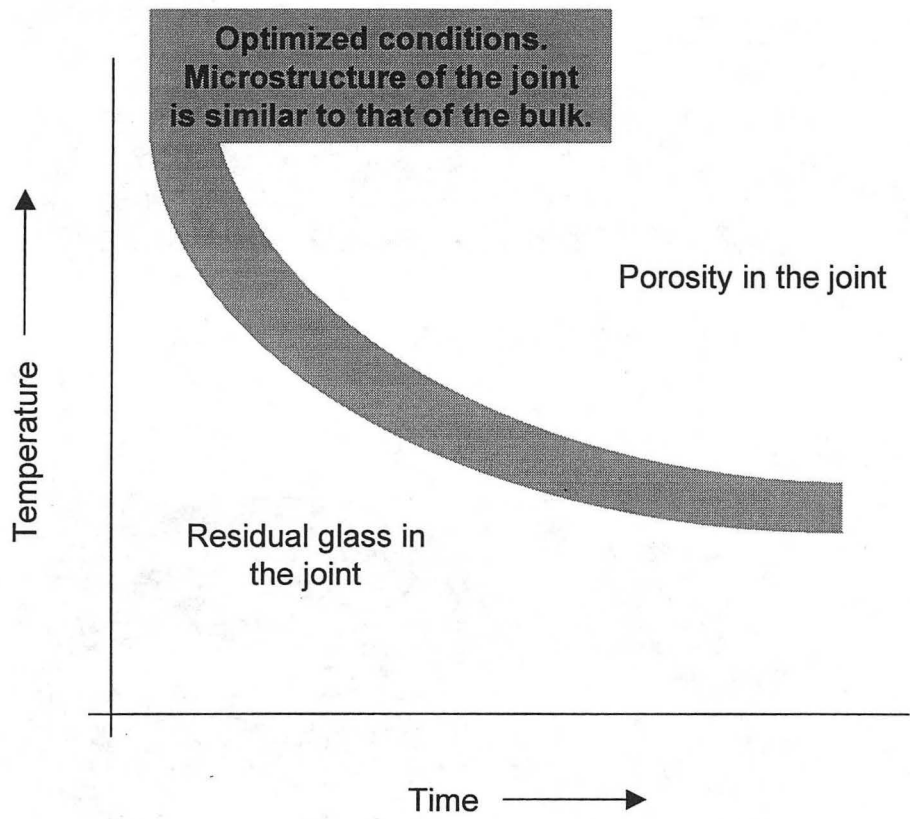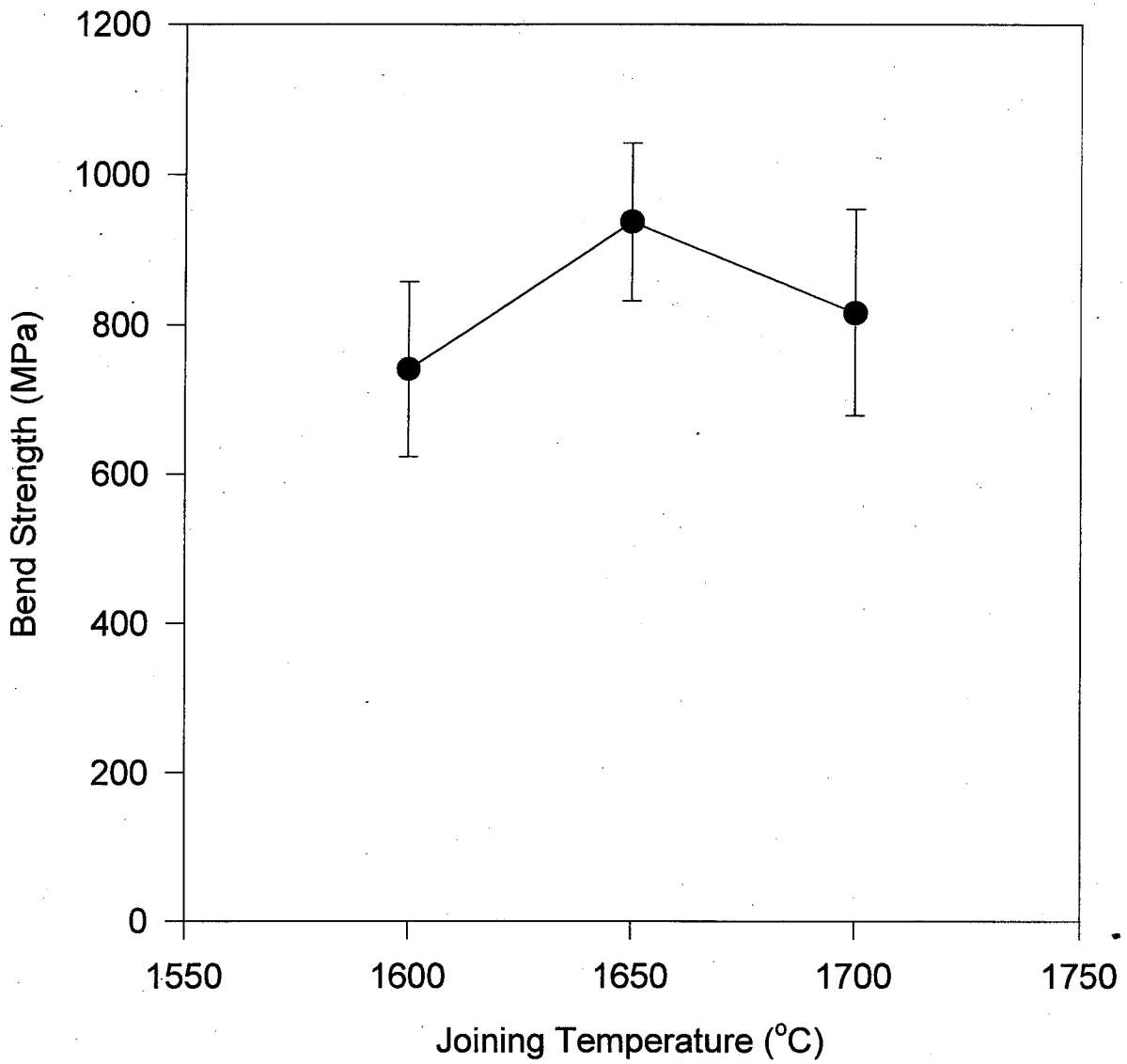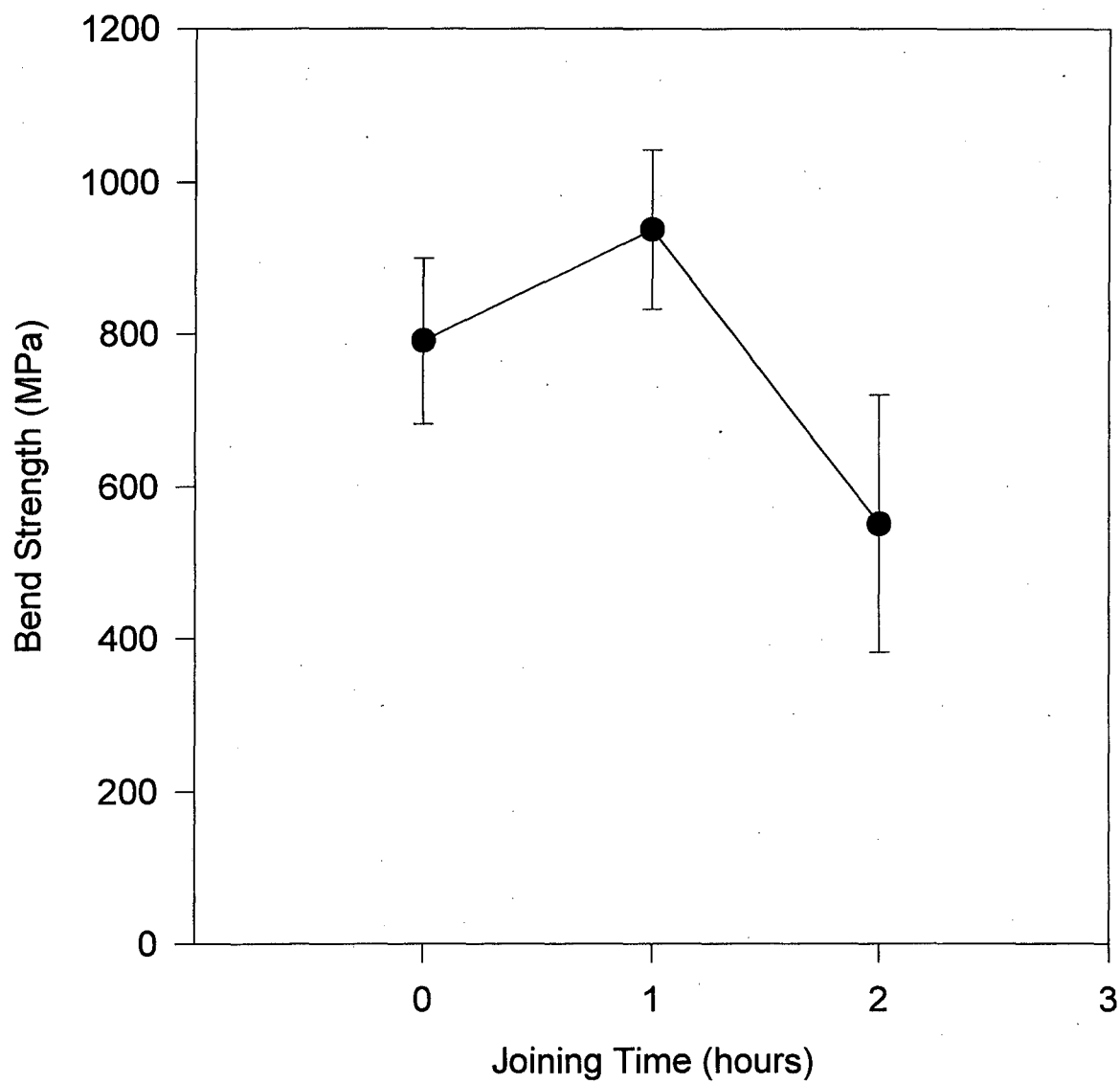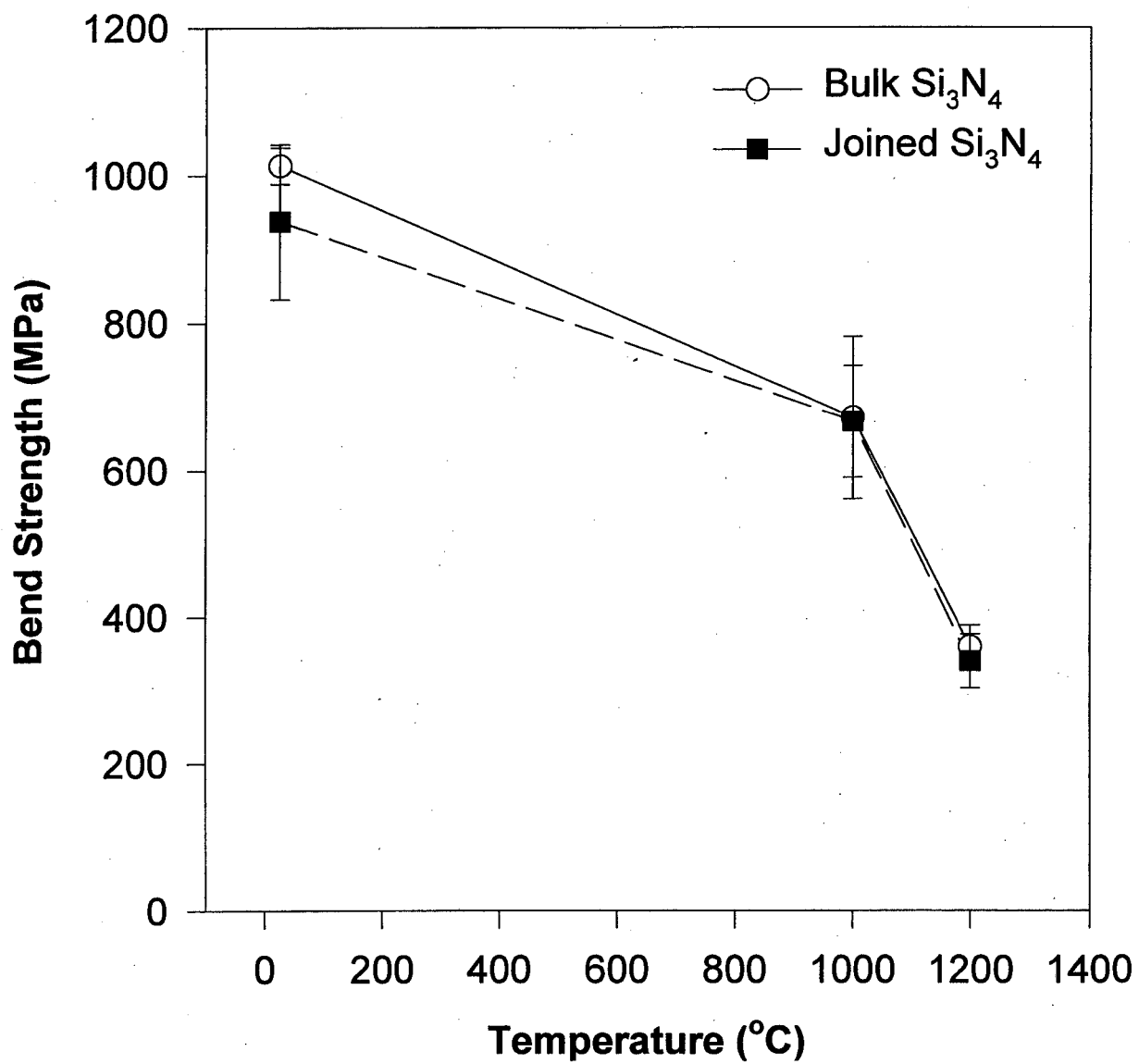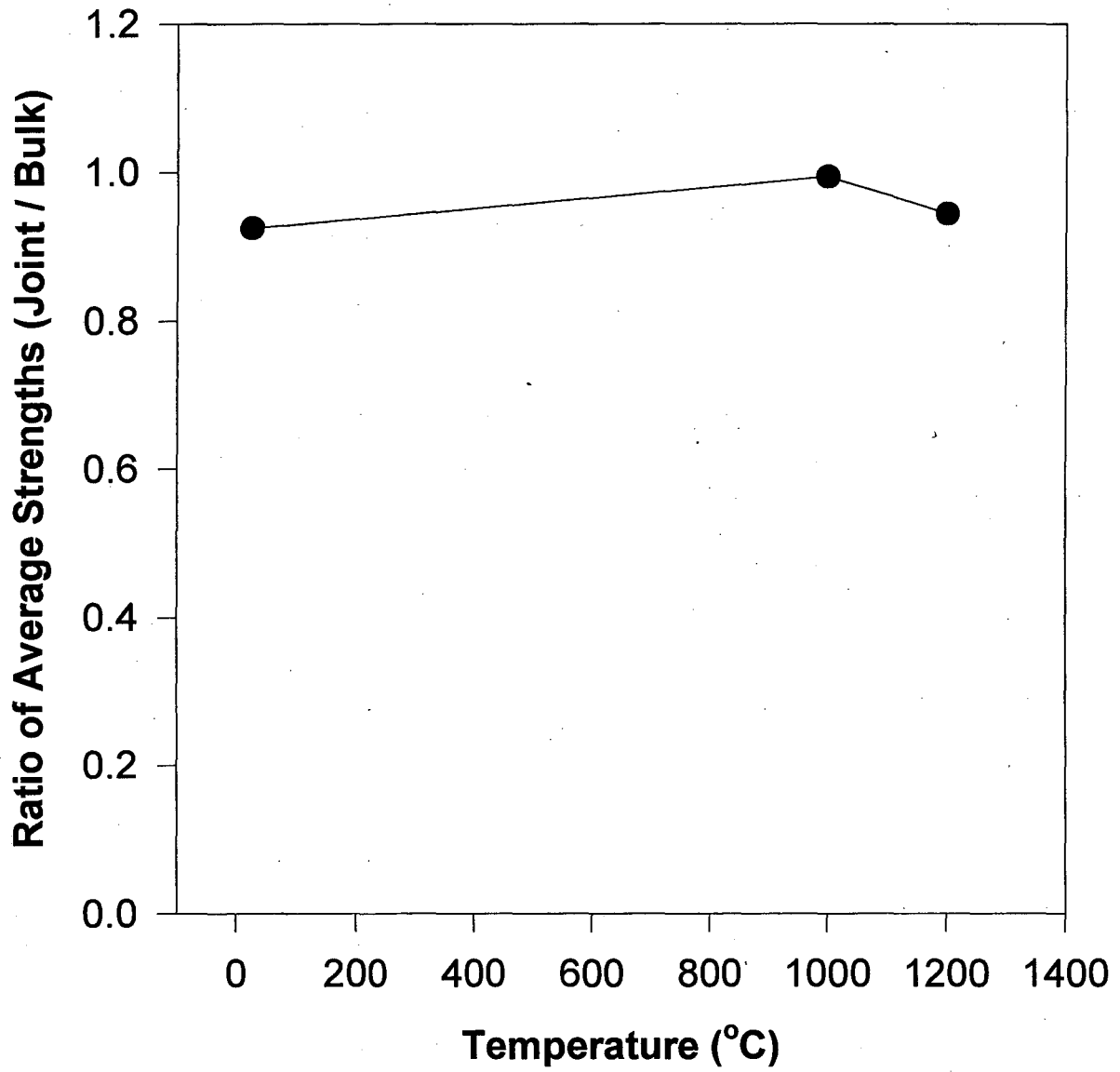
Figure 5 (c)

Figure 5 (d)

Figure 6

Figure 7

Figure 8

Figure 9

Figure 10